Journal of Neurology (2019) 266:2186–2196
https://doi.org/10.1007/s00415-019-09400-2

ORIGINAL COMMUNICATION

In vivo direct relation of tau pathology with neuroinflammation in early Alzheimer's disease

Tatsuhiro Terada[1,2] · Masamichi Yokokura[3] · Tomokazu Obi[2] · Tomoyasu Bunai[1] · Etsuji Yoshikawa[4] · Ichiro Ando[5] · Hitoshi Shimada[6] · Tetsuya Suhara[6] · Makoto Higuchi[6] · Yasuomi Ouchi[1]

Received: 4 April 2019 / Revised: 21 May 2019 / Accepted: 23 May 2019 / Published online: 28 May 2019

Abstract

Objective Neuronal damage and neuroinflammation are important events occurring in the brain of Alzheimer's disease (AD). The purpose of this study was to clarify in vivo mutual relationships among abnormal tau deposition, neuroinflammation and cognitive impairment in patients with early AD using positron emission tomography (PET) with [^{11}C]PBB3 and [^{11}C]DPA713.

Methods Twenty patients with early AD and 20 age-matched normal control (NC) subjects underwent a series of PET measurements with [^{11}C]PBB3 for tau aggregation and [^{11}C]DPA713 for microglial activation (neuroinflammation). Inter- and intrasubject comparisons were performed regarding the levels of [^{11}C]PBB3 binding potential (BP_{ND}) and [^{11}C]DPA713 BP_{ND} in the light of cognitive functions using statistical parametric mapping (SPM) and regions of interest (ROIs) method.

Results The [^{11}C]PBB3 BP_{ND} was greater in the temporo-parietal regions of AD patents than NC subjects, and a similar increasing pattern of [^{11}C]DPA713 BP_{ND} was observed in the same patients. Correlation analyses within the AD group showed a positive direct correlation between [^{11}C]PBB3 BP_{ND} and [^{11}C]DPA713 BP_{ND} in the parahippocampus. Pass analysis revealed that cognitive impairment was more likely linked to the level of the parahippocampal [^{11}C]PBB3 BP_{ND} than that of [^{11}C]DPA713 BP_{ND}.

Conclusions The pattern of abnormal tau deposition was very similar to that of neuroinflammation in patients with early-stage AD. Specifically, the direct positive correlation of tau pathology with neuroinflammation in the parahippocampus suggests that neuronal damage in this region is closely associated with microglial activation. Consistently, tau aggregation in this region matters more than neuroinflammation regarding the cognitive deterioration in AD.

Keywords Alzheimer's disease · TAU · Microglia · Positron emission tomography · [^{11}C]PBB3

✉ Yasuomi Ouchi
ouchi@hama-med.ac.jp

[1] Department of Biofunctional Imaging, Preeminent Medical Photonics Education and Research Center, Hamamatsu University School of Medicine, 1-20-1 Handayama Higashi-ku, Hamamatsu 431-3192, Japan

[2] Department of Neurology, Shizuoka Institute of Epilepsy and Neurological Disorders, Urushiyama 886, Aoi-ku, Shizuoka 420-8688, Japan

[3] Department of Psychiatry, Hamamatsu University School of Medicine, 1-20-1, Handayama, Higashi-ku, Hamamatsu 431-3192, Japan

[4] Central Research Laboratory, Hamamatsu Photonics KK, 5000 Hirakuchi, Hamakita-ku, Hamamatsu 4434-0041, Japan

[5] Hamamatsu PET Imaging Center, Hamamatsu Medical Photonics Foundation, Hirakuchi, Hamakita-ku, Hamamatsu 434-0041, Japan

[6] Department of Functional Brain Imaging Research, National Institute of Radiological Sciences, National Institutes for Quantum and Radiological Science and Technology, 4-9-1 Anagawa, Inage-ku, Chiba 263-8555, Japan

Introduction

The accumulation of senile plaques and neurofibrillary tangles are neuropathological hallmarks of Alzheimer disease (AD) [35]. Neuroinflammation is increasingly being recognized as playing a pivotal role in the pathology of AD [31, 37, 39]. Neuroinflammation in the AD brain is chiefly characterized by the presence of activated microglia [16, 37, 39]. The activated microglia accompany cerebral glucose hypometabolism or cerebral atrophy, suggesting that neuroinflammation predicts disease progression in patients with AD [6]. According to previous studies, β-amyloid (Aβ) accumulation activates microglia, which, in turn, accelerates Aβ accumulation by releasing inflammatory substances [16, 39]. However, our recent study did not support the theory that Aβ deposition itself accelerates microglial activation in AD [37]. According to the amyloid hypothesis, Aβ plays a key role in disease initiation [11, 12]. Aβ is responsible for triggering tau pathology, which is closely related to the progression of neurodegeneration [11, 30]. Neurodegeneration seems to be further accelerated in a vicious circle between activated microglia and tau pathology [3, 18]. Therefore, the link between activated microglia and aggregated tau is a key that must be considered when explaining the progression of AD. In the living AD brain, however, little is known about the mutual concurrent relationships among tau pathology, activated microglia and cognitive decline in the same patients. [^{11}C]PBB3 and [^{11}C]DPA713 were developed as PET tracers for aggregated tau [19, 30] and activated microglia [21, 22, 38], respectively. While molecular imaging studies of tau/neuroinflammation are flourishing, a large amount of data from different patients has been analyzed to determine biomarkers characterizing AD from the macroscopic perspective.

We aimed to assess the relationship between tau aggregation and neuroinflammation and their effects on clinical manifestations in the same group of patients with early AD using PET with [^{11}C]PBB3 and [^{11}C]DPA713.

Materials and methods

Participants

Twenty AD patients with clinical dementia rating (CDR) scores of 0.5 and 1 (7 men and 13 women; mean age ± SD: 69.4 ± 8.3 years, all right-handed) and twenty age-matched, normal control (NC) subjects (9 men, 11 women; 69.5 ± 8.8 years, all right-handed) were enrolled in this study. Patients and NC subjects were recruited from our hospital and by in-house advertisements, respectively, from April 2014 to April 2017. Participants were excluded if they had neurological problems that might interfere with cognitive function or MRI findings such as cerebrovascular disease, traumatic brain injury, brain tumor, hydrocephalus and epileptic foci. All patients met the criteria for the diagnosis of probable AD dementia with evidence of the AD pathophysiological process based on the criteria of National Institute on Aging-Alzheimer's Association workgroups on diagnostic guidelines for Alzheimer's Disease (NIA/AA AD) [1, 20]. Because we focused on the pathophysiological sign of early-stage AD in this study, patients with CDR 2 or 3 indicating severe or moderate dementia were excluded. All patients were scanned with [^{11}C]PiB PET within 6 months prior to the current study to biologically confirm the AD diagnosis [37]. This Aβ imaging was only used for selecting Aβ-positive AD patients. Indeed, the relation of Aβ with abnormal tau and neuroinflammation in the same platform might be interesting, but the considerable intervals between Aβ scans and others confound the outcome. All patients with AD were taking a minimum level of donepezil (5 mg) at entry because their clinical symptoms were mild, and the medications were temporarily suspended 12 h before the PET measurement to set the scan condition as uniformly as possible.

Neuropsychological assessments for all participants comprised the Mini-Mental State Examination (MMSE) for global cognitive function [34], Wechsler Memory Scale-Revised (WMSR) Logical Memory (LM) test for episodic memory, Frontal Assessment Battery (FAB) for executive function, and CDR for assessing the severity of symptoms of dementia.

This study was reviewed and approved by the Ethics Committee of Hamamatsu University School of Medicine and Hamamatsu Medical Center. Written informed consent was obtained from all subjects prior to participation in this study.

MRI scanning

Before the PET scan, MRI (1.5-T GE, Signa Excite HDx, Chicago, USA) of the brain was performed with 3-dimensional mode sampling (TR = 25.0, TE = minimum, flip angle 30°, slice thickness 1.5 mm, matrices 256 × 128, FOV = 24.0) to determine the brain areas in which to establish regions of interest (ROIs). With reference to the measures of tilt angle and spatial coordinates obtained in the procedure, which were used to determine the intercommissural [anterior commissure-posterior commissure (AC-PC)] line on the sagittal MRI of each subject's brain, a PET gantry was set parallel to the AC-PC line by tilting and moving the gantry for each study. The MRI measurements and mobile

PET gantry allowed us to reconstruct PET images parallel to the AC-PC line without reslicing.

PET data acquisition

For all participants, a series of PET measurements were performed after neuropsychological assessments using a high-resolution brain PET scanner (SHR12000; Hamamatsu Photonics K.K., Hamamatsu, Japan) [38]. A thermoplastic face mask was used to fix the head in the same place during the scans. Among the twenty NC subjects, four persons did not complete a 90-min [^{11}C]DPA713 scan of [^{11}C] DPA713 PET measurements due to a need to urinate. After a 10-min transmission scan for attenuation correction with a ^{68}Ge/^{68}Ga source, serial emission scans (frames captured in *n* seconds: 6 × 10, 3 × 20, 6 × 60, 4 × 180, and 14 × 300) were obtained for 90 min after a slow bolus venous injection (taking 1 min) of a 5 MBq/kg dose of [^{11}C]DPA713 (specific radioactivity > 108 GBq/μmol). After a 2.5-h rest, all participants underwent serial [^{11}C]PBB3 PET scans (frames captured in *n* seconds: 6 × 10, 3 × 20, 6 × 60, 4 × 180, and 10 × 300) for 70 min after a slow bolus venous injection (taking 1 min) of a 6 MBq/kg dose of [^{11}C] PBB3 (specific radioactivity > 105 GBq/μmol). No arterial sampling was performed along with the PET measurements.

Imaging data processing

It has been reported that [^{11}C]PBB3 delineates tau aggregation at the early stage in patients with AD [19, 30]. The BP_{ND} of [^{11}C]PBB3 was estimated with the simplified reference tissue model (SRTM) using PMOD 3.4 software (PMOD Technologies Ltd., Zurich, Switzerland) to assess tau deposition in the brain [15, 23]. In a series of reports with [^{11}C]PBB3, the cerebellum was chosen as a reference region for estimating the BP_{ND} of [^{11}C]PBB3 [25, 30]. These authors recently amended this method because the [^{11}C]PBB3 radioactivity in cerebellar ROIs suffers from overestimation by spillover or radioactivity from veins, resulting in underestimation of the BP_{ND} value [14]. Similar to this approach for detecting the lowest accumulation of [^{11}C]PBB3 in the intact brain in a segmentation manner, irregular ROIs were manually located bilaterally in the cerebellum (volume of interest: 0.88–2.42 cm^3), anterior cingulated cortex (5.03–7.46), caudate (1.23–3.36), putamen (3.06–7.04), thalamus (6.38–12.17), posterior cingulated cortex (0.79–3.27), precuneus (0.78–1.71), superior frontal cortex (4.76–7.34), middle frontal cortex (5.22–9.47), occipital cortex (0.49–1.03), lateral temporal cortex (4.04–7.71), medial temporal cortex (2.33–5.92) including hippocampus (0.81–1.94), parahippocampus (0.76–2.21), amygdala (0.75–2.07), parietal cortex (1.48–3.58), pons (4.00–9.08), and midbrain (2.88–5.45) on the brain MRI in reference to an MRI atlas [17]. We established irregular, small ROIs within the brain, including the pons, on MRI images of the brain and automatically on the corresponding [^{11}C]PBB3 parametric images and found that the pontine time activity curve (TAC) (rather than a conventional cerebellar TAC) was stable and exhibited the lowest intensity among TACs from multiple brain regions, including the cortex and subcortical regions. Based on the evidence that the brainstem is relatively spared from tau deposition in patients with AD until the late stage of the disease course [29], ROI data from the pons were adequate for determining the value of the reference region in the current study. Previous studies indicated that [^{11}C]PBB3 showed off-target binding in the dural venous sinuses and choroid plexus [9], spill-over radioactivity might affect the cerebellar TAC as described above. The extracerebral structures were masked out by demarcating cerebral regions on brain MRI.

Upon activation, microglia express increasing amounts of translocator protein (TSPO) on the outer mitochondrial membrane, and thus TSPO is a good marker of neuroinflammation in the brain [22]. Our recent TSPO PET study with a second-generation tracer [^{11}C]DPA713 showed greater merit of this tracer in terms of a higher affinity for TSPO than a conventional tracer, [^{11}C]DPA713, to depict neuroinflammation in the cerebral cortex [38]. Still, non-specific binding is supported to exist along with vessels, but non-specific binding was found to be significantly lower in almost all brain areas for [^{18}F]DPA714 (a second generation tracer of TSPO similar to the current [^{11}C]DPA713) compared to [^{11}C](*R*) PK11195 [10]. Despite the presence of polymorphisms for second-generation tracers, including [^{11}C]DPA713, Asian populations, unlike Caucasian populations, have a moderately homogenous pattern of its polymorphism (90% moderate binding affinity), allowing us to proceed with the present study without genetic testing (only Japanese people were recruited) [21, 38]. To assess the microglial activation in the brain, we estimated the BP_{ND} of [^{11}C]DPA713 with the SRTM as described elsewhere [33, 38]. A normalized input curve of [^{11}C]DPA713 was first created by averaging the TACs from the ROIs placed over the bilateral frontal, temporal, parietal and occipital cortices, thalamus, basal ganglia, cerebellar hemisphere, and brain stem in the control group. When applying the normalized mean TAC to the individual subjects to determine the individual reference input, this curve was calibrated by adjusting the lowest TAC peak from each subject based on a cluster analysis excluding the white matter and CSF space. The extracerebral structures were masked by demarcating cerebral regions on brain MRIs.

SPM analysis

To identify the regions that exhibit higher levels of [^{11}C] PBB3 BP_{ND} and [^{11}C]DPA713 BP_{ND} in patients with AD

than in NC subjects, we analyzed the whole brain using a voxelwise method with Statistical Parametric Mapping 8 software (SPM8; Wellcome Department of Imaging Neurosciences, London, UK; http://www.fil.ion.ucl.ac.uk/spm) running on MATLAB 7.12.0 (The MathWorks, Natick, MA, USA), which is still widely used in PET studies [38]. All [^{11}C]PBB3 and [^{11}C]DPA713 parametric BP_{ND} images were first normalized to the Montreal Neurological Institute (MNI) space using transformation parameters for early integrated image of [^{11}C]PBB3 from 0 to 20 min after injection and [^{11}C]DPA713 from 0 to 20 min after injection. After image normalization, all images were smoothed with an isotropic Gaussian kernel of 6 mm. Group comparisons were performed using two-sample t-tests in SPM8 to explore the regional differences in the [^{11}C]PBB3 or [^{11}C]DPA713 BP_{ND} between patients with AD (AD in total and AD at the CDR0.5) and the NC group using age and gender as covariates of no interest. The correlation analyses between PET biological and clinical parameters were conducted using an SPM multiple regression method. Because the test was exploratory in nature with a priori knowledge of locations of changes in tau deposition and microglial activation are known a priori, the significance was set to $p < 0.001$ at the voxel level (uncorrected for multiple regression).

The correlation analyses between [^{11}C]PBB3 BP_{ND} and MMSE score were conducted using an SPM multiple regression method. The significance was set to $p < 0.001$ at the voxel level (uncorrected for multiple regression).

ROI analysis

Regional BP_{ND} levels were determined from bilateral ROIs located in the parahippocampal region, medial temporal cortex including the hippocampal, entorhinal and parahippocampal regions, and lateral temporal cortex covering Brodmann areas 20–22 and 38 because these regions were particularly important as tau aggregation regions [5].

Since tau pathology initially develops in the medial temporal region [27, 28], we focused on this territory and divided it into two regions mentioned above to examine whether and where tau deposition within the temporal lobe was directly associated with microglial activation through a comparison of [^{11}C]PBB3 BP_{ND} with [^{11}C]DPA713 BP_{ND} from the same ROIs in all patients with AD using Spearman's correlation coefficients in the Statistical Package for Social Sciences version 16 (SPSS Inc., Chicago, IL, USA). Statistical significance was set to $p < 0.05$ with the Bonferroni correction. In the ROI analyses, we did not correct PET data for age and gender because neither age nor gender showed a significant difference between groups.

Path analyses among data for [^{11}C]PBB3 uptake, [^{11}C]DPA713 uptake and psychological test scores were performed in all patients with AD to illustrate the effects of these variables on each other [32]. In this analysis, path diagrams were designed, where the levels of [^{11}C]PBB3 BP_{ND} and [^{11}C]DPA713 BP_{ND} in those regions aforementioned, were separately compared to possible variables that are theoretically related as a cause or effect of clinical deteriorations (i.e., reductions in general cognition, logical memory and frontal executive function). Statistical significance was set at $p < 0.05$.

Results

Demographic and Clinical Characteristics

Demographic and AD-related clinical factors are presented in Table 1. Significantly lower mean scores on the MMSE, WMSR-LM-I + II, and FAB were recorded for patients with AD at CDR score of 1 than for patients with AD at CDR score of 0.5. No significant differences in the age and gender ratios were observed between the patients with AD and NC groups.

Table 1 Demographic and clinical characteristics of the Alzheimer's disease (AD) patient group and control groups

	Alzheimer's disease			Normal control	
	Total ($N = 20$)	CDR 0.5 ($N = 9$)	CDR 1 ($N = 11$)	[^{11}C]PBB3-PET ($N = 20$)	[^{11}C]DPA-PET ($N = 16$)
Age (years)	69.4 ± 8.3	71.7 ± 8.3	68.3 ± 8.5	69.5 ± 8.8	69.1 ± 9.0
Men/women (number)	7/13	4/5	3/8	9/11	6/10
Disease duration (years)	3.2 ± 1.6	2.7 ± 1.3	3.6 ± 1.8		
MMSE (/30)	22.3 ± 4.3	24.5 ± 4.2	18.5 ± 5.0	28.1 ± 2.1	27.8 ± 2.2
WMSR-LM-I + II (/100)	4.3 ± 5.4	5.5 ± 4.7	3.4 ± 5.6	24.0 ± 10.0	25.5 ± 10.5
FAB (/18)	9.5 ± 2.6	10.4 ± 2.8	8.1 ± 3.0	14.3 ± 2.3	14.3 ± 2.0

Data are presented as the mean ± SD (range)

CDR clinical dementia rating, *MMSE* Mini-Mental State Examination (normal level ≧ 24), *WMSR-LM-I + II* Wechsler Memory Scale-Revised Logical memory I + II (normal level ≧ 14), *FAB* frontal assessment battery (normal level ≧ 12)

Comparison of the [^{11}C]PBB3 BP_{ND} and [^{11}C]DPA713 BP_{ND} between the AD and Normal Groups

The SPM results showed that a significant increase in [^{11}C]PBB3 BP_{ND} was observed in the medial and lateral sides of the temporal and parietal lobes (Fig. 1a; Table 2), and that [^{11}C]DPA713 BP_{ND} was significantly increased in the temporal and parieto-occipital cortices in the same AD group (Fig. 1b; Table 3). The patterns of the elevation of binding of these tracers were apparently similar, which might at a glance allude simultaneous occurrence of abnormal tau and activated microglia in these regions.

Regarding the dementia severity or disease progression, significant increase in [^{11}C]PBB3 BP_{ND} [^{11}C]DPA713 BP_{ND} and was observed in rather limited areas covering the temporal and parietal cortices at the CDR 0.5 stage (Fig. 2).

Correlation between [^{11}C]PBB3 BP_{ND} and MMSE score

SPM analysis revealed that several clusters especially in the temporal and frontal cortices were identified as the regions in which MMSE score was negatively correlated with the [^{11}C]PBB3 BP_{ND} (Fig. 3).

Relationship Between [^{11}C]PBB3 BP_{ND} and [^{11}C]DPA BP_{ND} in the temporal lobe of AD group

A direct comparison between [^{11}C]PBB3 BP_{ND} and [^{11}C]DPA BP_{ND} in the same ROIs revealed a significant positive correlation in the parahippocampus ($R^2 = 0.400$, $p = 0.003$) (Fig. 4a), despite the tendency toward a positive correlation in the medial temporal and lateral temporal regions (Fig. 4b,2c).

The mutual correlations among [^{11}C]PBB3 BP_{ND}, [^{11}C]DPA713 BP_{ND} and neuropsychological scores

Since abnormal tau accumulation in the medial temporal region was related to microglial activation, we conducted a path analysis. The medial temporal [^{11}C]PBB3 BP_{ND} was a significant mediator of the [^{11}C]DPA BP_{ND} (beta coefficient = 0.42, $p = 0.049$, $R^2 = 0.18$) and MMSE score (beta coefficient = − 0.49, $p = 0.034$, $R^2 = 0.22$) (Fig. 5a). The indirect effect ($0.42\ x - 0.01 = 0.0042$) was so small that MMSE reduction was potentially unrelated to the change induced by tau-mediated neuroinflammation in the parahippocampus. Instead, the presence of tau itself in the area was a substantial effector of cognitive decline. In contrast, as shown in Fig. 2b, abnormal tau deposition in the lateral temporal cortex only correlated with MMSE reduction (beta coefficient = − 0.44, $p = 0.035$, $R^2 = 0.20$), but not microglial activation (Fig. 5b). Regarding the WMSR-LM scores, no significant correlation was observed in the light of the medial temporal tau load

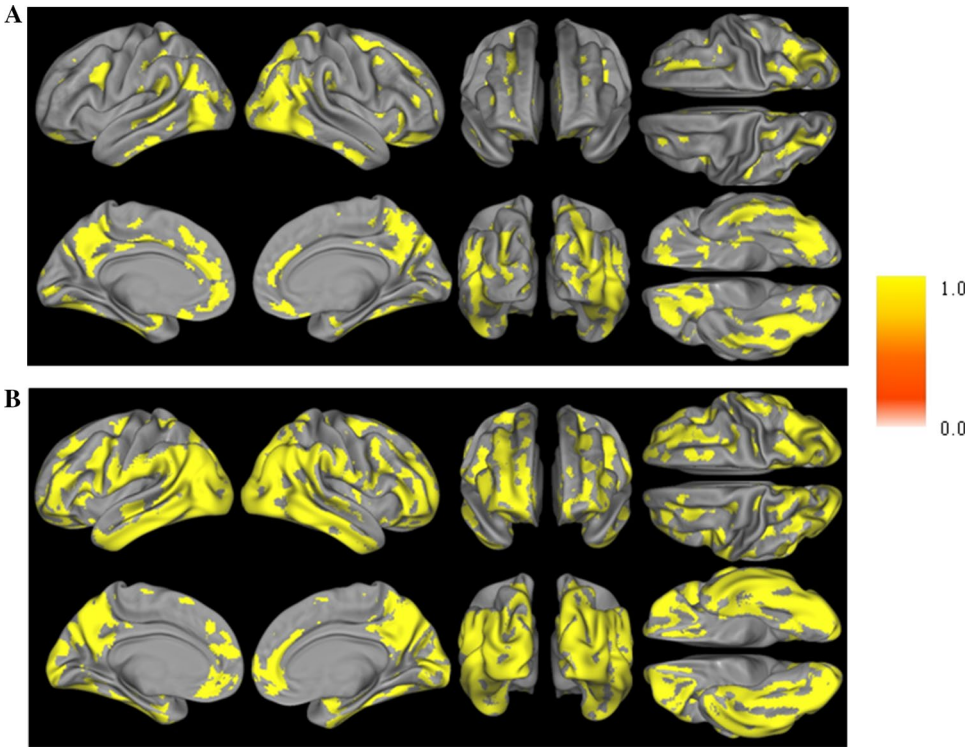

Fig. 1 Voxelwise results for [^{11}C]PBB3 and [^{11}C]DPA713 in the AD patients. The regions with significant elevation of [^{11}C]PBB3 BP_{ND} (**a**) and [^{11}C]DPA713 BP_{ND} (**b**). These surface-based pictures were proceeded using Caret software v5.65 (http://brainvis.wustl.edu/wiki/index.php/Caret:About). The color bar represents the *T* value

Table 2 Statistical parametric mapping (SPM) results on [^{11}C]PBB3 BP_{ND}

Anatomical region	BA	Talairach coordinate			Cluster size	Voxel *T* value	*Z* score	Cluster *p* value			Peak *p* value		
		x	*y*	*Z*				FWE	FDR	Uncorrected	FWE	FDR	Uncorrected
Right inferior frontal gyrus	47	33.7	32.7	− 6.7	30123	9.14	6.45	$p<0.001$	$p<0.001$	$p<0.001$	$p<0.001$	$p<0.001$	$p<0.001$
Left inferior parietal lobule	40	− 49.5	− 27.9	25.3		7.88	5.90				$p<0.001$	$p=0.002$	$p<0.001$
Right fusiform gyrus	20	29.7	− 37.8	− 18.3		7.83	5.88				$p<0.001$	$p=0.002$	$p<0.001$
Left insula	13	− 37.6	− 1.0	18.5	3834	6.51	5.21	$p<0.001$	$p<0.001$	$p<0.001$	$p=0.009$	$p=0.013$	$p<0.001$
Left orbital gyrus	11	− 7.9	41.7	− 20.6		6.21	5.04				$p=0.018$	$p=0.018$	$p<0.001$
Left anterior cingulate	24	− 9.9	30.1	18.8		5.53	4.64				$p=0.097$	$p=0.041$	$p<0.001$
Right medial frontal gyrus	6	13.9	− 17.1	46.9	20	4.13	3.69	$p=0.994$	$p=0.876$	$p=0.376$	$p=0.937$	$p=0.298$	$p<0.001$
Right lentiform nucleus		33.7	− 15.2	6.3	26	4.00	3.59	$p=0.985$	$p=0.876$	$p=0.311$	$p=0.974$	$p=0.369$	$p<0.001$
Left medial frontal gyrus	6	− 4.0	− 15.0	50.5	42	3.88	3.51	$p=0.933$	$p=0.876$	$p=0.201$	$p=0.991$	$p=0.438$	$p<0.001$
Left pyramis		− 9.9	− 79.0	− 26.3	24	3.83	3.47	$p=0.988$	$p=0.876$	$p=0.331$	$p=0.995$	$p=0.466$	$p<0.001$

BA Brodmann area; FWE, family-wise error; FDR, false discovery rate; AD, Alzheimer's disease

Table 3 Statistical Parametric Mapping (SPM) results on [^{11}C]DPA713 BP_{ND}

Anatomical region	BA	Talairach coordinate			Cluster size	Voxel *T* value	*Z* score	Cluster *p* value			Peak *p* value		
		x	*y*	*Z*				FWE	FDR	Uncorrected	FWE	FDR	Uncorrected
Right middle occipital gyrus	19	47.5	− 81.1	9.6	80826	7.62	6.14	$p<0.001$	$p<0.001$	$p<0.001$	$p<0.001$	$p=0.001$	$p<0.001$
Right middle temporal gyrus	39	37.6	− 68.6	27.4		7.56	6.11				$p<0.001$	$p=0.001$	$p<0.001$
Right angular gyrus	39	45.5	− 62.2	38.1		7.25	5.93				$p<0.001$	$p=0.001$	$p<0.001$
Left putamen		− 23.8	− 1.6	7.4	62	4.05	3.74	$p=0.843$	$p=0.799$	$p=0.185$	$p=0.824$	$p=0.235$	$p<0.001$
Right cingulate gyrus	32	13.9	9.6	36.4	21	3.85	3.58	$p=0.988$	$p=0.799$	$p=0.440$	$p=0.938$	$p=0.340$	$p<0.001$
Left superior frontal gyrus	6	− 2.0	14.3	52.7	70	3.75	3.50	$p=0.800$	$p=0.799$	$p=0.160$	$p=0.970$	$p=0.408$	$p<0.001$
Right lentiform nucleus		15.8	− 1.7	5.6	7	3.50	3.29	$p=0.999$	$p=0.799$	$p=0.674$	$p=0.998$	$p=0.656$	$p<0.001$
Left middle frontal gyrus	6	− 35.6	− 3.1	55.4	7	3.46	3.26	$p=0.999$	$p=0.799$	$p=0.674$	$p=0.999$	$p=0.704$	$p<0.001$
Left culmen of vermis		− 4.0	− 60.1	1.3	12	3.46	3.26	$p=0.997$	$p=0.799$	$p=0.568$	$p=0.999$	$p=0.705$	$p<0.001$
Right cingulate gyrus	31	17.8	− 29.1	40.1	10	3.44	3.23	$p=0.998$	$p=0.799$	$p=0.606$	$p=0.999$	$p=0.739$	$p<0.001$

BA Brodmann area, *FWE* family-wise error, *FDR* false discovery rate, *AD* Alzheimer's disease

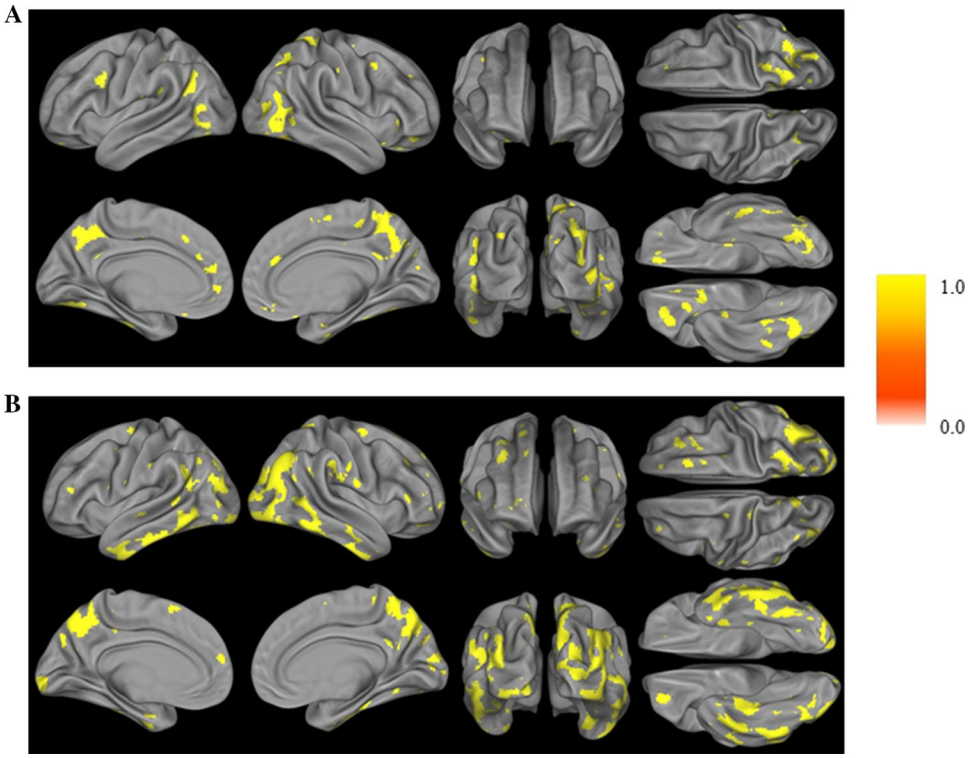

Fig. 2 Voxelwise results for [^{11}C]PBB3 and [^{11}C]DPA713 in the AD patients at CDR 0.5. The regions with significant elevation of [^{11}C]PBB3 BP_{ND} (**a**) and [^{11}C]DPA713 BP_{ND} (**b**)

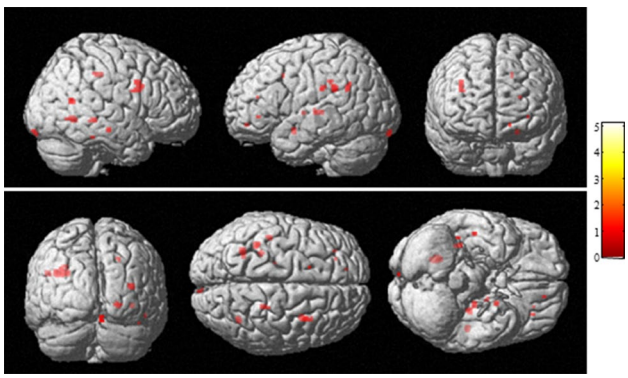

Fig. 3 Voxelwise results on the significant correlation of [^{11}C]PBB3 BP_{ND} and MMSE scores in AD patients. The color bar denotes the T-value

(Fig. 5c), whereas the beta coefficient (− 0.44) of lateral temporal tau load mediator to the level of WMSR-LM scores was significant ($p=0.032$, Fig. 5d). As for the FAB score, no correlation was found in the present path analysis.

Discussion

In the present study, our results showed significant increases in the levels of [^{11}C]PBB3 BP_{ND} in the temporo-parietal cortices and [^{11}C]DPA713 BP_{ND} in the seemingly similar brain regions in patients with early AD. Direct region-to-region comparisons highlighted the parahippocampus where these two PET parameters were significantly coupled with each other, suggesting the coexistence of tau pathology and neuroinflammation in this region, consistent with previous post-mortem pathological observations [13]. Furthermore, [^{11}C]PBB3 BP_{ND} within the medial temporal cortex including the parahippocampus, correlated significantly with the MMSE score, suggesting that tau pathology has a close relation with the reduction of general cognitive ability. However, based on the path analysis, the correlation between [^{11}C]DPA713 BP_{ND} in the parahippocampus and MMSE score was very weak, suggesting that tau-related neuroinflammation was not a bioindicator predicting general cognitive decline. Thus, the present results confirmed that tau pathology is surely a main culprit of cognitive impairment rather than neuroinflammation per se in patients with AD.

The present cross-sectional study did not allow clarification of the spread of abnormal tau in AD, but a categorization of AD patients into early- or moderate-stage groups would give a hint of the contention. As described in Table 1, we recruited patients at the CDR 0.5 and 1. Compared to the SPM results from the total AD patients, the brain regions showing higher levels of [^{11}C]PBB3 BP_{ND} were smaller in CDR-0.5 AD patients (Fig. 2a). While the number of CDR-0.5 patients was so small that this result was just preliminary, it can be extrapolated that the abnormal tau aggregation in vivo might reflect the distribution of fibrillar tau at Braak

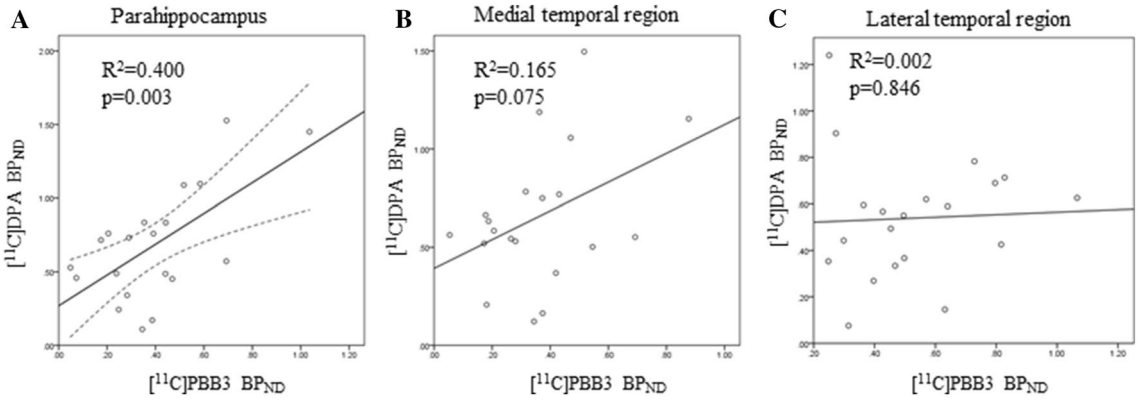

Fig. 4 Regions of interest-based multiple correlation analyses between [^{11}C]PBB3 BP_{ND} and [^{11}C]DPA713 BP_{ND} in the temporal lobe. **a** Parahippocampus, **b** medial temporal cortices, **c** lateral temporal cortices. Dotted lines represent 95% confidence intervals of the fitted lines in the scattergram

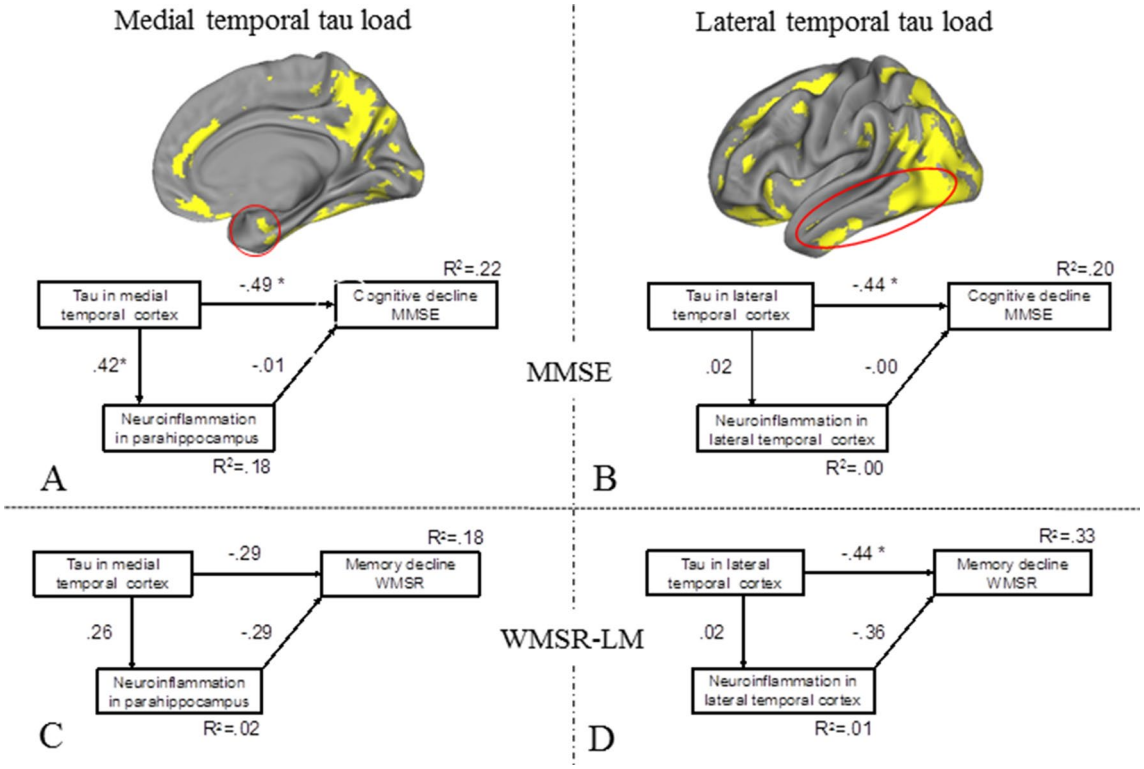

Fig. 5 Path diagrams among data for [^{11}C]PBB3 uptake, [^{11}C] DPA713 uptake and neuropsychological (MMSE and WMSR-LM) scores. **a** Tau deposition within the medial temporal cortex for MMSE, **b** tau deposition within the lateral temporal cortex for MMSE, **c** tau deposition within the medial temporal cortex for WMSR-LM, **d** tau deposition within the lateral temporal cortex for WMSR-LM. The asterisk indicates statistically significant. Likelihood ratio Chi squared: 8.013 *df* 3. Fit index: root mean error of approximation = 0.053

stages III–IV [7, 27, 29, 30], and hence the abnormal tau progression pattern might support the previous reports on Braak-based propagation of tau in patients with AD [27, 29].

Neuroinflammation is chiefly characterized by the presence of activated microglia [16, 31]. In ex vivo studies using animals and postmortem samples [16, 29], tau pathology sequentially induces neuroinflammation and neurodegeneration, and a long-lasting dementia period might determine the amount of aggregated tau in the human brain. Consistent with our previous report with [^{11}C](*R*)PK11195 [37], the level of [^{11}C]DPA713 BP_{ND} was increased throughout the brain in patients with AD. Of course, the distribution

of tracer uptake looked different between the current result and the previous one because PET tracers and the degree of dementia severity were different. A use of [^{11}C]DPA713 in the current study was found more advantageous to visualize microglial activation than the first-developed TSPO tracer [^{11}C](*R*)PK11195 because [^{11}C]DPA713 has been shown to detect minimal changes in microglial activation especially in an Asian population [21, 37, 38]. The pattern of elevation of [^{11}C]DPA713 binding looked similar across the total AD patients, but the extent of the binding was shown to be smaller in AD patients at CDR 0.5 (Fig. 2b).

A combination of [^{11}C]PBB3 and [^{11}C]DPA713 will likely provide additional information that was lacking in our previous study (Aβ and neuroinflammation) [38]. In the current study, we did not deal with [^{11}C]PIB data for Aβ accumulation because the timing of [^{11}C]PIB scan was so separate from the dates of [^{11}C]PBB3/[^{11}C]DPA713 scans performed on the same day. As illustrated in Fig. 1, it seems that the cluster of regions with significantly elevated [^{11}C]PBB3 BP_{ND} would overlap with the multiple regions in which [^{11}C]DPA BP_{ND} was significantly increased. The current direct region-to-region comparisons in the temporal lobe the reportedly tau aggregation territory found early in AD [12] highlighted the parahippocampus as an area of close linkage between tau aggregation and neuroinflammation. It has been reported that tau pathology exists in the medial temporal lobe [27, 30] during age, followed by medial temporal lobe atrophy and memory impairments [27]. This pathophysiology occurring during the aging process is recognized as primary age-related tauopathy (PART) or a part of the AD spectrum [27]. Since neuroinflammation occurs regardless of the disease or aging [38], activated microglia that contribute to the development of tau pathology and its progression in the AD brain [18] would have a detrimental effect on the neuronal environment in AD. Indeed, the present result that [^{11}C]PBB3 accumulation positively correlates with [^{11}C]DPA713 binding in the parahippocampus in early AD patients gives in vivo evidence that abnormal tau burden in the medial temporal region is responsible for an acceleration of microglial activation.

As shown in Fig. 3, one theory can be deduced from the path analysis regarding the significance of mutual relations among tau aggregation, neuroinflammation and cognitive impairment. In the early stage of AD, medial temporal (parahippocampal) tau accumulation directly correlated with general cognitive dysfunction evaluated by MMSE or an endophenotype of neurodegeneration [2] and neuroinflammation. In Fig. 3, voxel-wise evaluation revealed significant brain regions with tau deposition that correlated negatively with MMSE scores, showing its dominancy in the medial temporal regions. These findings support the hypothesis that tau pathology is tightly associated with the deterioration of cognitive ability in patients with AD in the clinical setting [7, 24, 27]. It was reported that neuroinflammation assessed by [^{11}C](*R*)PK11195 in the lateral temporal region was associated with cognitive decline in AD [6], our recent study failed to show a significant correlation between [^{11}C]DPA713 binding and MMSE [38]. This might be ascribed to the different severity of disease, different regions of focus, or different population of TSPO polymorphism. The lack of significant correlation about memory function assessed by WMSR-LM might be due to the stage of the disease; there might be a chance of positive correlation between abnormal tau deposition in this region and memory deterioration if adults with subjective or mild cognitive impairment or preclincal AD were recruited. Not only postmortem but also in vivo evaluations of the AD brain show that abnormal tau accumulates from the medial temporal to lateral neocortical areas [4, 19]. Considering this spread of tau aggregation, tau pathology in the lateral temporal cortex would have some adverse effects on cognition. Indeed, the path analysis showed that both scores (MMSE and WMSR-LM) were negatively correlated with tau accumulation in the lateral temporal cortex (Fig. 5b, d). Since microglia are easily activated by various factors, including misfolded proteins such as Aβ and tau, impairing neuronal function and networking and subsequently affecting homeostasis [8, 26, 36], microglial activation seemingly concurring with abnormal tau accumulation may be ascribed to this susceptibility of microglia in the AD brain.

Several limitations must be mentioned. The sample size was relatively small, but the power analysis with a δ (mean difference) of 0.12 and σ (SD) of 0.13 from the other sets of AD groups in a preliminary study generated a sample size of 19, allowing us to perform the study. Since the current study did not employ a longitudinal design but was cross-sectional in nature, information on within-subject changes in these pathophysiological biomarkers is not available. Since Aβ accumulation can activate microglia, a comparative study is needed to clarify how much amyloid deposition contributes to microglial activation in the same region. The lack of medical intervention, such as anti-Aβ/anti-tau antibodies or anti-neuroinflammatory agents, in this study prevents us from disclosing the cause-and-effect relationship between tau deposition and microglial activation in the living brains of patients with AD. Although Japanese people have been reported to have a moderately homogenous pattern of polymorphisms for TSPO, a lack of genetic testing for TSPO polymorphisms is one of limitations in our study. There is a chance that patients with low or high affinity might have been included.

Conclusion

The current study shows that tau pathology in the parahippocampus is linked with neuroinflammation, which induces general cognitive deterioration in AD patients.

Neuroinflammation that would graphically coincide with tau aggregation in the lateral temporal cortex and possibly in other brain regions might be caused by many factors that disrupt the brain milieu other than tau pathology in AD.

Acknowledgements We thank Mr. Toshihiko Kanno and the staff of Hamamatsu Medical Photonics Foundation and Hamamatsu Photonics K.K. for their valuable technical assistance.

Author contributions TT designed and performed the research, analyzed the data, and wrote the paper. MY, TO, TB, EY performed the research. IA synthesized tracers. HS, TS and MH interpreted the data. YO designed and conceptualized the research and wrote the paper.

Funding This study was supported by the Japanese Ministry of Education, Culture, Sports, Science and Technology (16H06402A01, 17H042470001), Japan Agency for Medical Research and Development (16768966), Grant-in-Aid for Research and Development Grants for Dementia (16768966) from the Japan Agency for Medical Research and Development (AMED).

Compliance with ethical standards

Conflicts of interest Authors TT, MY, TO, TB, EY, IA and YO declare no competing interests. HS, TS and MH hold patent on compounds related to the present report (JP 5422782/EP 12 884 742.3), and the National Institutes for Quantum and Radiological Science and Technology made a license agreement with APRINOIA Therapeutics Inc. regarding this patent.

References

1. Albert MS, DeKosky ST, Dickson D, Dubois B, Feldman HH, Fox NC, Gamst A, Holtzman DM, Jagust WJ, Petersen RC, Snyder PJ, Carrillo MC, Thies B, Phelps CH (2011) The diagnosis of mild cognitive impairment due to Alzheimer's disease: recommendations from the National Institute on Aging-Alzheimer's Association workgroups on diagnostic guidelines for Alzheimer's disease. Alzheimer's Dementia J Alzheimer's Assoc 7:270–279
2. Annicchiarico R, Federici A, Pettenati C, Caltagirone C (2007) Rivastigmine in Alzheimer's disease: cognitive function and quality of life. Ther Clin Risk Manag 3:1113–1123
3. Asai H, Ikezu S, Tsunoda S, Medalla M, Luebke J, Haydar T, Wolozin B, Butovsky O, Kugler S, Ikezu T (2015) Depletion of microglia and inhibition of exosome synthesis halt tau propagation. Nat Neurosci 18:1584–1593
4. Braak H, Braak E (1991) Neuropathological stageing of Alzheimer-related changes. Acta Neuropathol 82:239–259
5. Braak H, Del Tredici K (2012) Alzheimer's disease: pathogenesis and prevention. Alzheimer's Dementia J Alzheimer's Assoc 8:227–233
6. Cagnin A, Brooks DJ, Kennedy AM, Gunn RN, Myers R, Turkheimer FE, Jones T, Banati RB (2001) In-vivo measurement of activated microglia in dementia. Lancet 358:461–467
7. Carlson JO, Gatz M, Pedersen NL, Graff C, Nennesmo I, Lindstrom AK, Gerritsen L (2015) Antemortem prediction of braak stage. J Neuropathol Exp Neurol 74:1061–1070
8. Cerami C, Iaccarino L, Perani D (2017) Molecular imaging of neuroinflammation in neurodegenerative dementias: the role of in vivo PET imaging. Int J Mol Sci 18:993
9. Chiotis K, Stenkrona P, Almkvist O, Stepanov V, Ferreira D, Arakawa R, Takano A, Westman E, Varrone A, Okamura N, Shimada H, Higuchi M, Halldin C, Nordberg A (2018) Dual tracer tau PET imaging reveals different molecular targets for (11)C-THK5351 and (11)C-PBB3 in the Alzheimer brain. Eur J Nucl Med Mol Imag 45:1605–1617
10. Doorduin J, Klein HC, Dierckx RA, James M, Kassiou M, de Vries EF (2009) [11C]-DPA-713 and [18F]-DPA-714 as new PET tracers for TSPO: a comparison with [11C]-(R)-PK11195 in a rat model of herpes encephalitis. Mol Imag Biol 11:386–398
11. Guggenberger R, Fischer DR, Metzler P, Andreisek G, Nanz D, Jacobsen C, Schmid DT (2013) Bisphosphonate-induced osteonecrosis of the jaw: comparison of disease extent on contrast-enhanced MR imaging, [18F] fluoride PET/CT, and conebeam CT imaging. AJNR Am J Neuroradiol 34:1242–1247
12. Hardy JA, Higgins GA (1992) Alzheimer's disease: the amyloid cascade hypothesis. Science 256:184–185
13. Jefferies WA, Food MR, Gabathuler R, Rothenberger S, Yamada T, Yasuhara O, McGeer PL (1996) Reactive microglia specifically associated with amyloid plaques in Alzheimer's disease brain tissue express melanotransferrin. Brain Res 712:122–126
14. Kimura Y, Endo H, Ichise M, Shimada H, Seki C, Ikoma Y, Shinotoh H, Yamada M, Higuchi M, Zhang MR, Suhara T (2016) A new method to quantify tau pathologies with (11)C-PBB3 PET using reference tissue voxels extracted from brain cortical gray matter. EJNMMI Res 6:24
15. Kimura Y, Ichise M, Ito H, Shimada H, Ikoma Y, Seki C, Takano H, Kitamura S, Shinotoh H, Kawamura K, Zhang MR, Sahara N, Suhara T, Higuchi M (2015) PET quantification of tau pathology in human brain with 11C-PBB3. J Nucl Med 56:1359–1365
16. Li Y, Tan MS, Jiang T, Tan L (2014) Microglia in Alzheimer's disease. Biomed Res Int 2014:437483
17. JrK Mai, Assheuer J, Paxinos G (1997) Atlas of the human brain. Academic Press, San Diego
18. Maphis N, Xu G, Kokiko-Cochran ON, Jiang S, Cardona A, Ransohoff RM, Lamb BT, Bhaskar K (2015) Reactive microglia drive tau pathology and contribute to the spreading of pathological tau in the brain. Brain 138:1738–1755
19. Maruyama M, Shimada H, Suhara T, Shinotoh H, Ji B, Maeda J, Zhang MR, Trojanowski JQ, Lee VM, Ono M, Masamoto K, Takano H, Sahara N, Iwata N, Okamura N, Furumoto S, Kudo Y, Chang Q, Saido TC, Takashima A, Lewis J, Jang MK, Aoki I, Ito H, Higuchi M (2013) Imaging of tau pathology in a tauopathy mouse model and in Alzheimer patients compared to normal controls. Neuron 79:1094–1108
20. McKhann GM, Knopman DS, Chertkow H, Hyman BT, Jack CR Jr, Kawas CH, Klunk WE, Koroshetz WJ, Manly JJ, Mayeux R, Mohs RC, Morris JC, Rossor MN, Scheltens P, Carrillo MC, Thies B, Weintraub S, Phelps CH (2011) The diagnosis of dementia due to Alzheimer's disease: recommendations from the National Institute on Aging-Alzheimer's Association workgroups on diagnostic guidelines for Alzheimer's disease. Alzheimer's Dementia J Alzheimer's Assoc 7:263–269
21. Owen DR, Yeo AJ, Gunn RN, Song K, Wadsworth G, Lewis A, Rhodes C, Pulford DJ, Bennacef I, Parker CA, StJean PL, Cardon LR, Mooser VE, Matthews PM, Rabiner EA, Rubio JP (2012) An 18-kDa translocator protein (TSPO) polymorphism explains differences in binding affinity of the PET radioligand PBR28. J Cereb Blood Flow Metab 32:1–5
22. Papadopoulos V, Baraldi M, Guilarte TR, Knudsen TB, Lacapere JJ, Lindemann P, Norenberg MD, Nutt D, Weizman A, Zhang MR, Gavish M (2006) Translocator protein (18 kDa): new nomenclature for the peripheral-type benzodiazepine receptor based on its structure and molecular function. Trends Pharmacol Sci 27:402–409

23. Passamonti L, Vazquez Rodriguez P, Hong YT, Allinson KS, Williamson D, Borchert RJ, Sami S, Cope TE, Bevan-Jones WR, Jones PS, Arnold R, Surendranathan A, Mak E, Su L, Fryer TD, Aigbirhio FI, O'Brien JT, Rowe JB (2017) 18F-AV-1451 positron emission tomography in Alzheimer's disease and progressive supranuclear palsy. Brain 140:781–791
24. Pontecorvo MJ, Devous MD Sr, Navitsky M, Lu M, Salloway S, Schaerf FW, Jennings D, Arora AK, McGeehan A, Lim NC, Xiong H, Joshi AD, Siderowf A, Mintun MA (2017) Relationships between flortaucipir PET tau binding and amyloid burden, clinical diagnosis, age and cognition. Brain 140:748–763
25. Saint-Aubert L, Lemoine L, Chiotis K, Leuzy A, Rodriguez-Vieitez E, Nordberg A (2017) Tau PET imaging: present and future directions. Mol Neurodegener 12:19
26. Sarlus H, Heneka MT (2017) Microglia in Alzheimer's disease. J Clin Invest 127:3240–3249
27. Scholl M, Lockhart SN, Schonhaut DR, O'Neil JP, Janabi M, Ossenkoppele R, Baker SL, Vogel JW, Faria J, Schwimmer HD, Rabinovici GD, Jagust WJ (2016) PET imaging of Tau deposition in the aging human brain. Neuron 89:971–982
28. Schonheit B, Zarski R, Ohm TG (2004) Spatial and temporal relationships between plaques and tangles in Alzheimer-pathology. Neurobiol Aging 25:697–711
29. Serrano-Pozo A, Frosch MP, Masliah E, Hyman BT (2011) Neuropathological alterations in Alzheimer disease. Cold Spring Harb Perspect Med 1:a006189
30. Shimada H, Kitamura S, Shinotoh H, Endo H, Niwa F, Hirano S, Kimura Y, Zhang MR, Kuwabara S, Suhara T, Higuchi M (2017) Association between Abeta and tau accumulations and their influence on clinical features in aging and Alzheimer's disease spectrum brains: a [11C]PBB3-PET study. Alzheimers Dement (Amst) 6:11–20
31. Spangenberg EE, Lee RJ, Najafi AR, Rice RA, Elmore MR, Blurton-Jones M, West BL, Green KN (2016) Eliminating microglia in Alzheimer's mice prevents neuronal loss without modulating amyloid-beta pathology. Brain 139:1265–1281
32. Stage FKCH, Nora A (2004) Path analysis: an introduction and analysis of a decade of research. J Educ Res 98:5–13
33. Terada T, Yokokura M, Yoshikawa E, Futatsubashi M, Kono S, Konishi T, Miyajima H, Hashizume T, Ouchi Y (2016) Extrastriatal spreading of microglial activation in Parkinson's disease: a positron emission tomography study. Ann Nucl Med 30:579–587
34. Tombaugh TN, McIntyre NJ (1992) The mini-mental state examination: a comprehensive review. J Am Geriatr Soc 40:922–935
35. Trojanowski JQ, Lee VM (2000) "Fatal attractions" of proteins. A comprehensive hypothetical mechanism underlying Alzheimer's disease and other neurodegenerative disorders. Ann N Y Acad Sci 924:62–67
36. Tronel C, Largeau B, Santiago Ribeiro MJ, Guilloteau D, Dupont AC, Arlicot N (2017) Molecular targets for PET imaging of activated microglia: the current situation and future expectations. Int J Mol Sci 18:802
37. Yokokura M, Mori N, Yagi S, Yoshikawa E, Kikuchi M, Yoshihara Y, Wakuda T, Sugihara G, Takebayashi K, Suda S, Iwata Y, Ueki T, Tsuchiya KJ, Suzuki K, Nakamura K, Ouchi Y (2011) In vivo changes in microglial activation and amyloid deposits in brain regions with hypometabolism in Alzheimer's disease. Eur J Nuclear Med Mol Imaging 38:343–351
38. Yokokura M, Terada T, Bunai T, Nakaizumi K, Takebayashi K, Iwata Y, Yoshikawa E, Futatsubashi M, Suzuki K, Mori N, Ouchi Y (2017) Depiction of microglial activation in aging and dementia: positron emission tomography with [11C]DPA713 versus [11C](R)PK11195. J Cereb Blood Flow Metab 37:877–889
39. Zhang F, Jiang L (2015) Neuroinflammation in Alzheimer's disease. Neuropsychiatr Dis Treat 11:243–256